

## Article

# Performance of Novel Antimicrobial Protein Bg\_9562 and In Silico Predictions on Its Properties with Reference to Its Antimicrobial Efficiency against *Rhizoctonia solani*

Pranathi Karnati <sup>1,†</sup>, Rekha Gonuguntala <sup>1,†</sup>, Kalyani M. Barbadikar <sup>1,†</sup>, Divya Mishra <sup>1</sup>, Gopaljee Jha <sup>2</sup>, Vellaisamy Prakasham <sup>1</sup>, Priyanka Chilumula <sup>1</sup>, Hajira Shaik <sup>1</sup>, Maruthi Pesari <sup>1</sup>, Raman Meenakshi Sundaram <sup>1,\*</sup> and Kannan Chinnaswami <sup>1,\*</sup> 

<sup>1</sup> Department of Pathology, Indian Institute of Rice Research, Hyderabad 500030, India; pranathi05@gmail.com (P.K.); rekha.bt89@gmail.com (R.G.); kalyaniaau@gmail.com (K.M.B.); mishradivya04@gmail.com (D.M.); vprakasam.iari@gmail.com (V.P.); cpriyanka2456@gmail.com (P.C.); hmasoodsk@gmail.com (H.S.); pesari.maruthi@gmail.com (M.P.)

<sup>2</sup> Plant Microbe Interactions Lab, National Institute of Plant Genome Research, Aruna Asaf Ali Marg, New Delhi 110067, India; jmsgopal@gmail.com

\* Correspondence: rms\_28@rediffmail.com (R.M.S.); agrikannan@gmail.com (K.C.)

† These authors contributed equally to this work.

**Abstract:** Bg\_9562 is a potential broad-spectrum antifungal effector protein derived from the bacteria *Burkholderia gladioli* strain NGJ1 and is effective against *Rhizoctonia solani*, the causal agent of sheath blight in rice. In the present study, in vitro antifungal assays showed that Bg\_9562 was efficient at 35 °C and 45 °C and ineffective either at high acidic pH (3.0) or alkaline pH (9.5) conditions. Compatibility studies between the native bioagents *Trichoderma asperellum* TAIK1 and *Bacillus subtilis* BIK3 indicated that Bg\_9562 was compatible with the bioagents. A field study using foliar spray of the Bg\_9562 protein indicated the need of formulating the protein before its application. In silico analysis predicted that Bg\_9562 possess 111 amino acid residues (46 hydrophobic residues, 12 positive and 8 negative residues) with the high aliphatic index of 89.92, attributing to its thermostability with a half-life of 30 h. Bg\_9562 (C<sub>491</sub>H<sub>813</sub>N<sub>137</sub>O<sub>166</sub>S<sub>5</sub>) possessed a protein binding potential of 1.27 kcal/mol with a better possibility of interacting and perturbing the membrane, the main target for antimicrobial proteins. The secondary structure revealed the predominance of random coils in its structure, and the best 3D model of Bg\_9562 was predicted using an ab initio method with Robetta and AlphaFold 2. The predicted binding ligands were nucleic acids and zinc with confidence scores of 0.07 and 0.05, respectively. The N-terminal region (1–14 residues) and C-terminal region (101 to 111) of Bg\_9562 residues were predicted to be disordered regions. Stability and binding properties of the protein from the above studies would help to encapsulate Bg\_9562 using a suitable carrier to maintain efficiency and improve delivery against *Rhizoctonia solani* in the most challenging rice ecosystem.

**Keywords:** antifungal protein; sheath blight; biological control; in silico analysis; protein modeling



**Citation:** Karnati, P.; Gonuguntala, R.; Barbadikar, K.M.; Mishra, D.; Jha, G.; Prakasham, V.; Chilumula, P.; Shaik, H.; Pesari, M.; Sundaram, R.M.; et al. Performance of Novel Antimicrobial Protein Bg\_9562 and In Silico Predictions on Its Properties with Reference to Its Antimicrobial Efficiency against *Rhizoctonia solani*. *Antibiotics* **2022**, *11*, 363. <https://doi.org/10.3390/antibiotics11030363>

Academic Editor: Ludger Ständker

Received: 25 January 2022

Accepted: 3 March 2022

Published: 8 March 2022

**Publisher's Note:** MDPI stays neutral with regard to jurisdictional claims in published maps and institutional affiliations.



**Copyright:** © 2022 by the authors. Licensee MDPI, Basel, Switzerland. This article is an open access article distributed under the terms and conditions of the Creative Commons Attribution (CC BY) license (<https://creativecommons.org/licenses/by/4.0/>).

## 1. Introduction

Management of plant pathogens using alternate methods to chemical pesticides, in the present era of consumer awareness and climate change, is a necessity more than an option. Pesticide residues are a major issue of concern in the domestic and export markets, affecting the overall income and livelihood of farmers. In this context, antagonistic microbes offer an alternative for a wide range of inputs, for such alternative eco-friendly strategies of pest and disease management [1]. Antimicrobial metabolites and proteins from the microbes offer numerous opportunities to manage the plant pathogens effectively, provided they are used appropriately [2]. These compounds are highly sensitive to environmental conditions, in particular temperature, light and moisture, and therefore need special formulations to

be more viable and effective during storage, handling and in field applications [3]. There are several reports on the utilization of formulated antifungal proteins for the treatment of human infections, mostly from the prospects of drug discovery and target delivery against human pathogens [4]. Antifungal (AF) proteins in general are classified into groups based on their mode of action. The first group, which are generally amphipathic in nature, act by lysis [5], while the second group interferes with cell wall synthesis or biosynthesis of essential components such as glucan or chitin [6,7]. Use of fungal-derived antifungal and bacterial-derived antifungal proteins for the management of plant pathogens has been extensively reviewed [8].

Rice (*Oryza sativa* L.) is one of the two principal food crops in India. India is the second-largest producer, consumer and exporter, with an average production of 117.47 mT in an area of 43.79 mha [9]. The average yield losses in rice due to pests and diseases vary between 10–30% depending on the severity of the stress factors involved [10]. Among other diseases, sheath blight disease is one of the most destructive, leading to a significant yield reduction in rice [11]. Sheath blight disease of rice is caused by soil-born fungi, *Rhizoctonia solani* (RS) (Basidiomycetes; teleomorph: *Thanatephorus cucumeris*), which attacks more than 100 host plants [11]. The fungus is divided into 14 anastomosis groups (AG1 to AG13 and AGB1) among which the subgroup AG1 IA is the most common cause of disease in at least 27 families of monocots and dicots [12,13]. Currently, the disease is largely managed by the application of chemical fungicides [14]. As there is an increasing concern regarding pesticide residues in crop products and soils, non-chemical disease control is becoming increasingly popular [15], and in addition, the integrated approach with the use of biocontrol agents would reduce the chances of pathogens evolving resistance against the fungicides [16].

Recently, a prophage tail-like protein produced by the bacteria *Burkholderia gladioli* strain NGJ1 named Bg\_9562 was demonstrated to have microphagous activity against RS using a Type III secretion system (T3SS; Injectisome) effector protein for entering the fungal hyphae [17]. Bg\_9562 and its various orthologs were found to harbor a conserved phage\_TAC\_7 superfamily domain and no known toxic or lytic domain was detected in Bg\_9562 and its orthologs [17]. Despite being very effective against RS, the physicochemical properties, 3D structure, mode of action as an antifungal agent and its translocation in the plant system still remain to be investigated. To address this issue, the current study is focused on identifying different properties of Bg\_9562 through wet-lab experiments with RS and coupled with in silico computational approaches to predict the 3D structure of the protein for obtaining insights regarding the structural and functional characterization of the protein. We obtained the purified protein from NIPGR (National Institute of Plant Genome Research, New Delhi, India) and conducted the wet-lab in vitro assays and field studies. The physicochemical properties, transmembrane regions, and thermal stability-related residues of the protein were determined in silico and correlated with wet-lab experiments and bioactivity assays of Bg\_9562 on RS. The interaction of Bg\_9562 with potential native biocontrol agents *Trichoderma asperellum* TAIK1 and *Bacillus subtilis* BIK3 [18] was studied, which helps in the use of this protein along with the biocontrol agents. In summary, this study aims to identify the antimicrobial properties of Bg\_9562 for its effective usage as a biocontrol agent to fight against sheath blight disease of rice.

## 2. Results

### 2.1. Antifungal Efficacy of Bg\_9562 on RS

The purified protein was found to be suppressing the growth of RS in vitro when compared to the control. In the experiment on different treatments of protein and *R. solani* under different temperature and pH conditions, it was observed that the protein was effective at both the temperature variables (35 °C, 45 °C) and ineffective at acidic pH (3.0). It was effective in restricting mycelial growth even with increased temperatures, indicating its thermal stability (Figure 1). However, it was inactive and unable to restrict the mycelial growth at either acidic or alkaline pH but effective under neutral pH (Table S1).

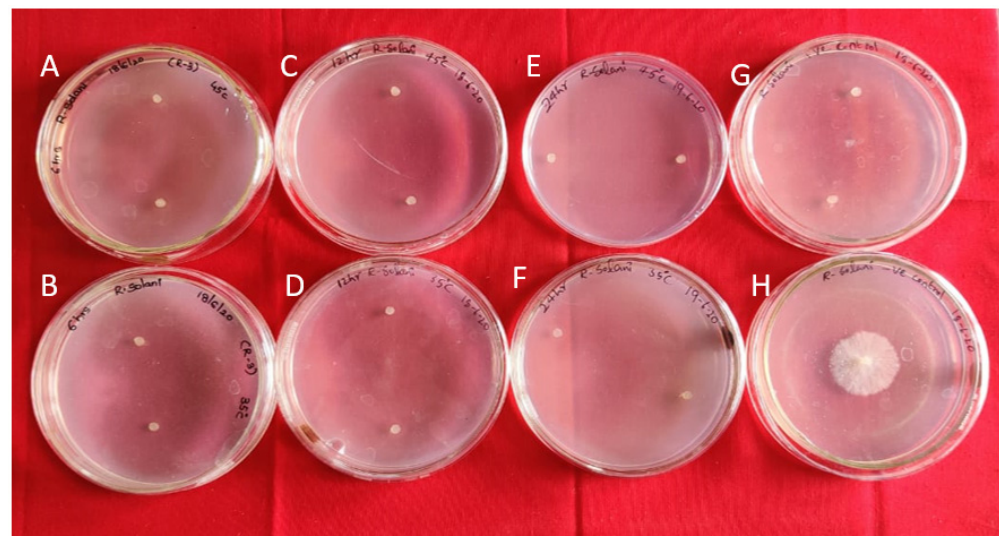


**Figure 1.** Antifungal activity of Bg\_9562 protein at varied temperatures and incubation periods (*R. solani* mycelial discs): (A,B) 6 h incubation at 45 °C, 35 °C; (C,D) 12 h incubation at 45 °C, 35 °C; (E,F) 24 h incubation at 45 °C, 35 °C; (G) untreated protein (positive control); (H) *R. solani* (negative control). Observations taken after 24 h.

## 2.2. In Vitro Compatibility of Bioagents, *Trichoderma Asperellum* TAIK1 and *Bacillus Subtilis* BIK3 with Bg\_9562

In vitro studies indicated that Bg\_9562 has no adverse effect on the growth of these bioagents, at both the temperature variables (35 °C, 45 °C) at different time intervals (6 h, 12 h and 4 h), and were able to grow normally (Figures 2 and 3). No inhibition in growth was observed in the antagonistic microbes tested, even after 7 days of incubation.

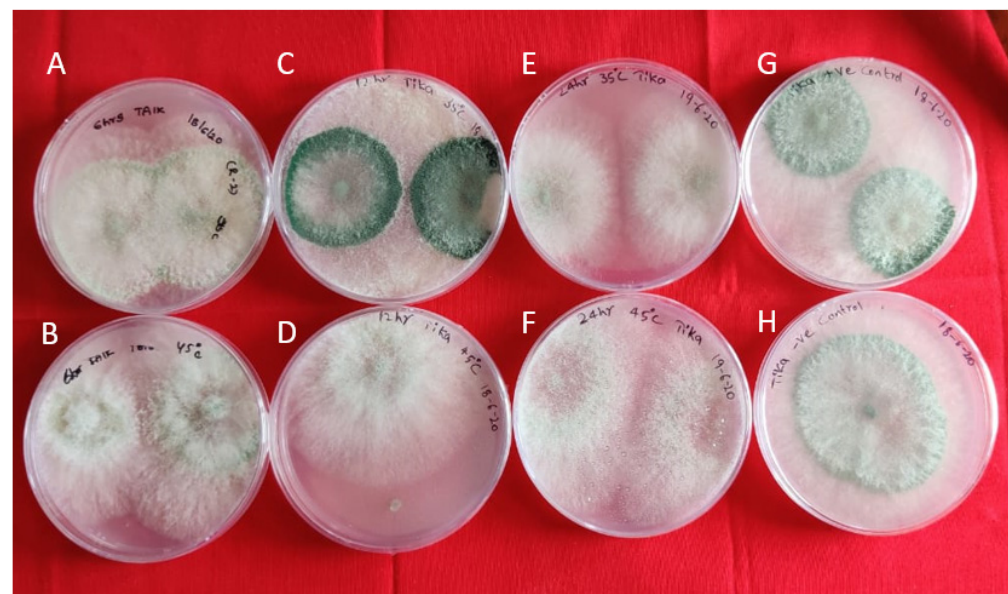


**Figure 2.** Interaction of Bg\_9562 protein and TAIK1 mycelial discs at varied temperatures and incubation periods: (A,B) 6 h incubation at 45 °C, 35 °C; (C,D) 12 h incubation at 45 °C, 35 °C; (E,F) 24 h incubation at 45 °C, 35 °C; (G) untreated protein (positive control); (H) TAIK1 (negative control); no effect of protein on mycelial growth. Observations taken after 24 h.

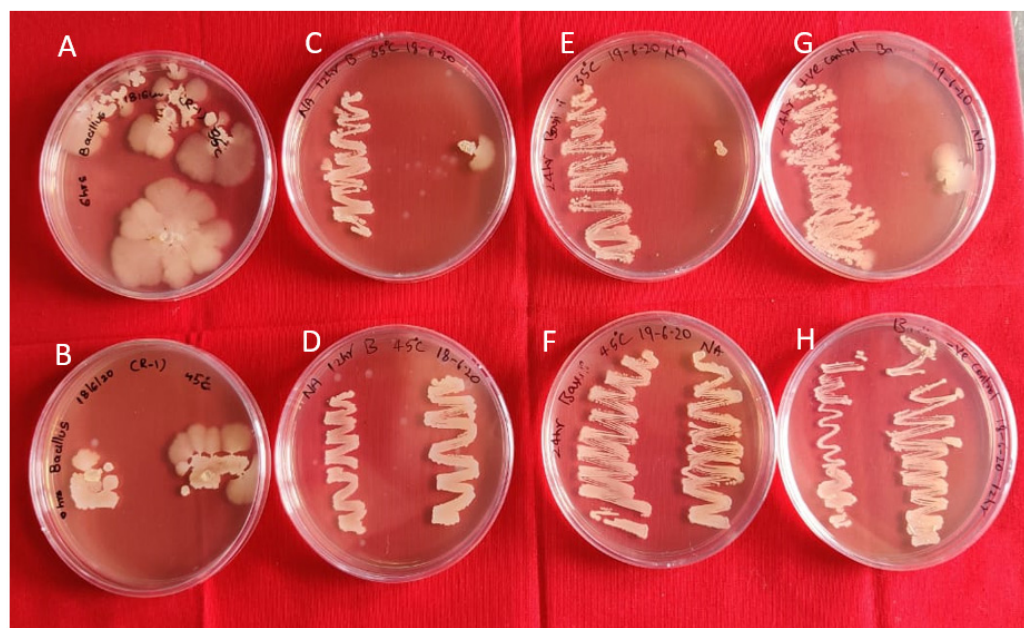


**Figure 3.** Antifungal activity of Bg\_9562 protein and BIK3 colony discs at varied temperatures and incubation periods: (A,B) 6 h incubation at 45 °C, 35 °C; (C,D) 12 h incubation at 45 °C, 35 °C; (E,F) 24 h incubation at 45 °C, 35 °C; (G) untreated protein (positive control); (H) BIK3 (negative control); no effect of protein on bacterial growth. Observations taken after 24 h.

### 2.3. Assessment of Bg\_9562 Protein Activity under Field Conditions

Data recorded in the field revealed that direct foliar treatment of plants with Bg\_9562 was not efficient to manage the disease incidence, calculated as percentage disease index (PDI) in comparison to the positive control (Table S2). From the results obtained, it can be assumed that direct foliar spray may be ineffective in controlling the disease; however, formulating the protein along with compatible biocontrol agents may be effective against RS.

### 2.4. Amino Acid Composition in Bg\_9562

The Bg\_9562 protein sequence contains 111 amino acids (Table S3) as predicted using the ExPasy-translate online application (Table S4). In silico studies on amino acid composition revealed that the Bg\_9562 protein has the maximum alanine (14.4%) and minimum cysteine (0.9%) and histidine (0.9%) residues (Table S5). A complete absence of two aromatic amino acids, tryptophan and tyrosine was observed. The total number of negatively-charged residues (Asp + Glu) was 12 and the total number of positively-charged residues (Arg + Lys) was 8, while the total number of hydrophobic amino acids (Ile + Val + Leu + Phe + Cys + Met + Ala + Tyr) was 46.

### 2.5. Physicochemical Properties of Bg\_9562 Determined Using ProtParam Tool

The molecular weight of Bg\_9562 was predicted to be 11.5 kDa and its theoretical isoelectric point was calculated as 4.65. The total net charge was estimated as  $-3.75$  at neutral pH, indicating that Bg\_9562 has an acidic nature. Further, Bg\_9562 was found to be a stable protein with the predicted instability index value of 21.19 (Table 1). The aliphatic index of Bg\_9562 was estimated to be as high as 89.92. The GRAVY (grand average of hydropathicity) index of Bg\_9562 was predicted to be  $-0.012$ , indicating the solubility of the protein and its hydrophilic nature. The estimated half-life of Bg\_9562 was 30 h. The extinction coefficient was estimated as  $0 \text{ M}^{-1} \text{ cm}^{-1}$  at 280 nm measured in water, assuming all cysteine residues are reduced and converted to cystines. Due to the absence of tryptophan residue in the Bg\_9562 protein, the estimation could result in more than 10% error in the computed extinction coefficient.

**Table 1.** List of physicochemical properties of Bg\_9562 protein using ProtParam tool.

S. No	Parameters	Values/Scores
1	Number of amino acids	111
2	Molecular weight	11,451.97
3	Theoretical isoelectric point	4.65
4	Total number of negatively-charged residues (Asp + Glu)	12
5	Total number of positively-charged residues (Arg + Lys)	8
6	Total number of hydrophobic amino acids (Ile + Val + Leu + Phe + Cys + Met + Ala + Tyr)	46
7	Total number of atoms	1612
8	Formula	C <sub>491</sub> H <sub>813</sub> N <sub>137</sub> O <sub>166</sub> S <sub>5</sub>
9	Instability index	21.19
10	Aliphatic index	89.92
11	Grand average of hydropathicity index (GRAVY)	−0.012
12	Estimated half-life (mammalian reticulocytes, in vitro)	30 h
13	Estimated half-life (yeast, in vitro)	>20 h
14	Estimated half-life ( <i>Escherichia coli</i> , in vivo)	>10 h
15	Extinction coefficient	0 M <sup>−1</sup> cm <sup>−1</sup>

### 2.6. Physicochemical Properties of Bg\_9562 Determined Using ProtScale

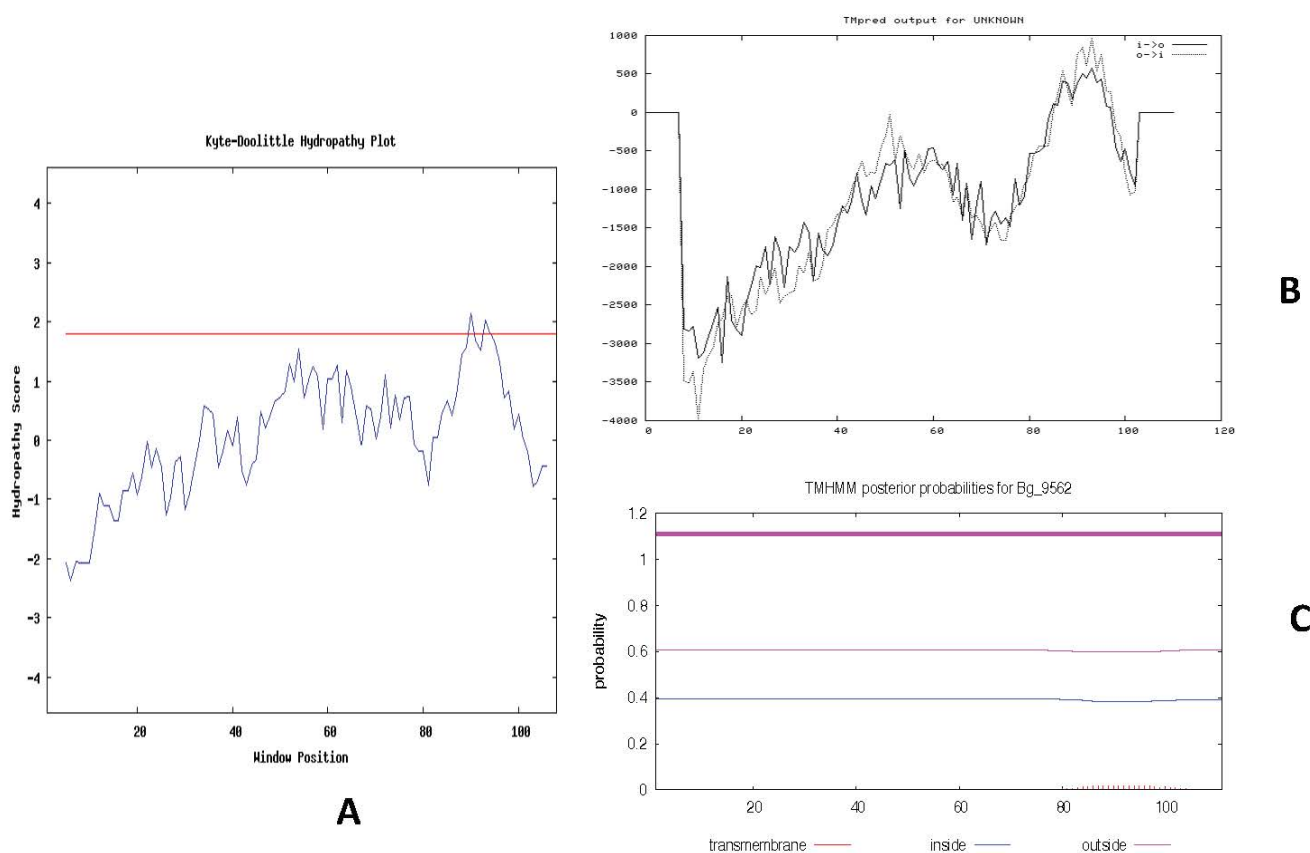
The details of other important physicochemical properties of Bg\_9562 are provided in Table S6. These were predicted using the ExPASy-ProtScale tool (Table S4) with a default window size of 9 and values obtained were normalized so that they all fit in the range of 0 to 1.

### 2.7. Bg\_9562 Properties Determined Using APD

Using predictive tools available at Antimicrobial Peptide Database v2.34, it was found that Bg\_9562 has antimicrobial activity (Table 2). The Boman index [19] estimated the protein binding potential of Bg\_9562 as 1.27 kcal/mol, which indicates the potential affinity of Bg\_9562 with other proteins in the cell. A higher Boman index value (>2.48) indicates that a given antimicrobial protein will be multifunctional or will play a variety of different roles within the cell due to its ability to interact with a wide range of proteins, while a low or negative Boman index value indicates a less effective antimicrobial protein. Another tool at APD, which estimated the hydrophobicity if the amino acid contributed favorably to membrane interface partitioning of peptides, was determined by the Wimley–White scale for interfacial insertions. Interestingly, Bg\_9562 displayed a high Wimley–White whole-residue hydrophobicity value of 26.18 kcal/mol, indicating that it is hydrophobic. Furthermore, it indicated that it has a better possibility of interacting and perturbing the membrane, which is the main target of action of many antimicrobial proteins. A hydropathy plot drawn using the Kyte and Doolittle scale (Table S4) (Figure 4A) predicted hydrophobic regions with a single transmembrane region in Bg\_9562. Similar results were obtained with hydrophobicity (Kyte and Doolittle) estimated using the ProtScale tool (Table S6), indicating the hydrophobic nature of Bg\_9562. The transmembrane nature of Bg\_9562 was determined using TMPred (Transmembrane Predictor) software and TMHMM-2.0 server (prediction of transmembrane helices in protein). Both the tools detected a single transmembrane region in the protein Bg\_9562 between 83 to 102 amino acid positions (Figure 4B,C).

**Table 2.** List of various parameters of Bg\_9562 predicted using Antimicrobial Peptide Database (APD)-based prediction.

S. No.	Parameter	Values
1	Protein binding potential (Boman index)	1.27 kcal/mol
2	The Wimley–White whole-residue hydrophobicity of the peptide	26.18 kcal/mol
3	APD defined total hydrophobic ratio of protein	41%
4	Total net charge	−3.75
5	Antimicrobial activity	Yes

**Figure 4.** Hydrophathy plot constructed for Bg\_9562 protein and prediction of transmembrane region of Bg\_9562. (A) Kyte–Doolittle hydrophathy plot was constructed with 103 effective amino acids and with the window size of 9. The peaks above the red line (~1.8) in the graph indicate possible transmembrane regions in the protein. (B) The output of TMpred analysis shows presence of single strong transmembrane helices with 83–102 residues of Bg\_9562 protein. (C) Prediction of transmembrane region with high probability using TMHMM software.

### 2.8. Propensity of Crystallization

Bg\_9562 was found to crystallize with a 0.507 confidence score by the CRYSTALP2 webserver. This server generates the predictions utilizing the composition and collocation of amino acids, isoelectric point, and hydrophobicity, as estimated from the primary sequence of the given protein. Similar results were obtained with the PPCpred webserver (predictor of protein production, purification and crystallization), where the crystallization was with the propensity value of 0.23. A PPCpred predicted score of above 0.4 has the ability to crystallize the protein, thus suggesting a difficulty in crystallization of Bg\_9562.

### 2.9. Sub-Program Sorting Using PSORT Tool

The possible cleavage site of Bg\_9562 was estimated between 56 and 57 amino acid residues. It was noticed that no N-terminal signal peptide, no endoplasmic reticulum retention site and no peroxisomal targeting signal were present in the C-terminal region. There was no possible vacuolar targeting motif and no RNA-binding motif likewise. Similarly, there was no transport motif from the cell surface to Golgi, and no N-myristoylation pattern was found. Therefore, the  $\kappa$ -nearest neighbor ( $\kappa$ -NN) algorithm was deployed for assessing the probability of localizing at each candidate site, where  $\kappa$  is a predefined integer parameter. A two-fold  $\kappa$ -NN was employed by the PSORT tool (Protein Subcellular Localization Prediction tool), where two different  $\kappa$  values ( $\kappa_1 < \kappa_2$ ) were used, localization sites were classified into two categories according to their data size, and the prediction probability for localization corresponded to the reckoned  $\kappa$ -data points. The results showed that  $\kappa$ -data points contained nuclear proteins with 47.8%, cytoplasmic proteins with 34.8%, mitochondrial proteins with 8.7% and cytoskeleton proteins with 8.7%. The Bg\_9562 was predicted to be localized in the nucleus with a probability of 47.8%.

### 2.10. Secondary Structure of Bg\_9562

Secondary structure prediction of Bg\_9562 using various methods of the NPS@ (Network Protein Sequence @analysis) server estimated that there is a dominance of coiled structural components followed by helices and extended strands in Bg\_9562 (Table 3). Similar results were also obtained using PSIPRED 4.0 workbench (PSIBLAST-based secondary structure PREDiction) (Figure 5A,B).

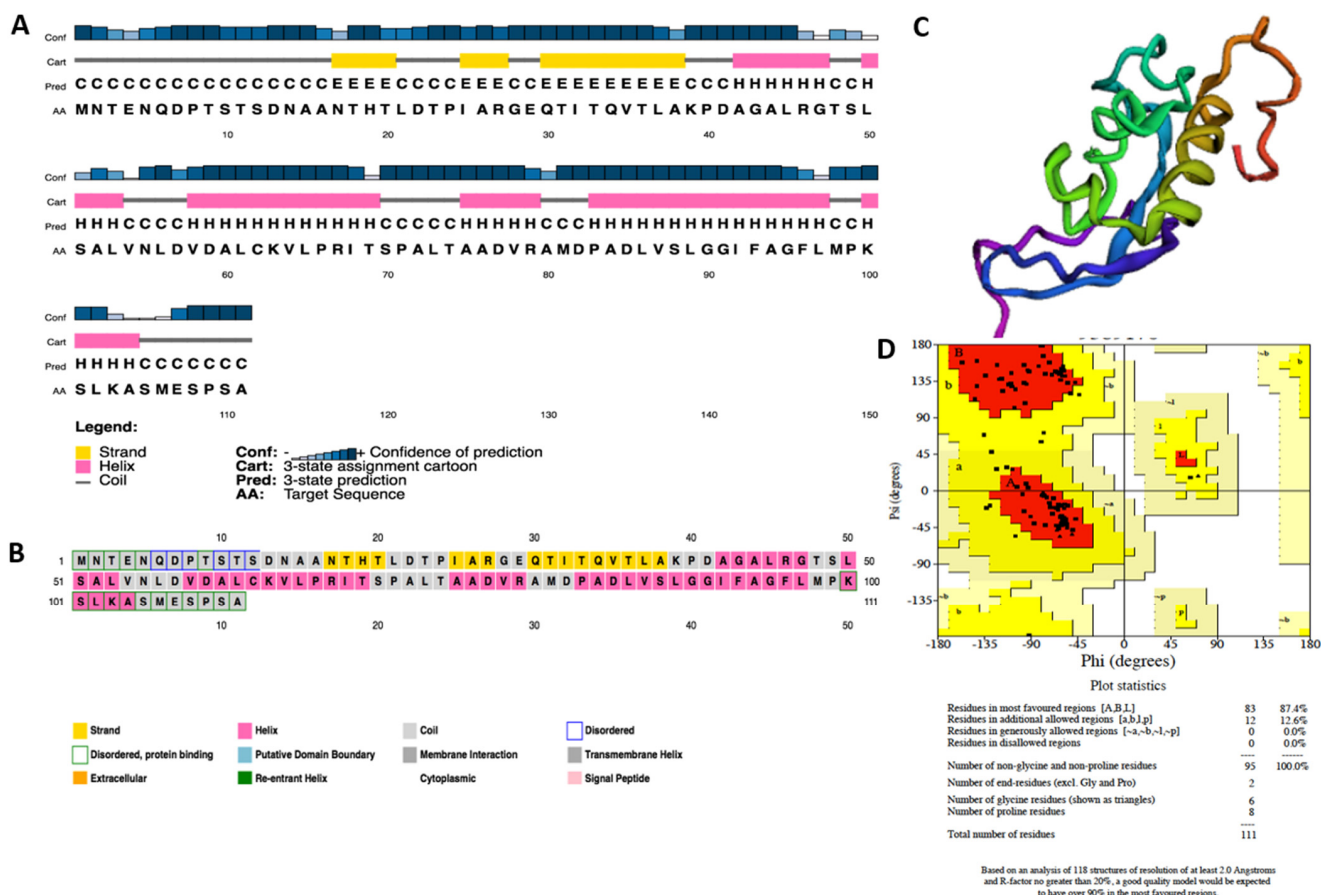


**Figure 5.** (A) Prediction of secondary structure of Bg\_9562 using PSIPRED 4.0 work bench (B) Annotation grid showing the structure and function of each residue of Bg\_9562 protein using PSIPRED 4.0. (C) 3D structure model of Bg\_9562 developed using Robetta (D) Validation of 3D structure model using Ramachandran plot.

**Table 3.** Secondary structure of Bg\_9562 predicted using NPS@ server.

Secondary Structure	DSC *	HNN *	MLRC *	PHD *	PREDATOR	Secondary Consensus
Alpha helix	55.86%	27.3%	26.13%	34.23%	22.52%	36.04%
Extended strand	3.6%	7.21%	9.91%	16.22%	3.6%	9.91%
Random coil	40.54%	65.77%	63.96%	49.55%	73.87%	52.25%

\* DSC—Discrimination of Protein Secondary structure Class. \* HNN—Hierarchical Neural Network method. \* MLRC—Multivariate Linear Regression Combination. \* PHD—Prediction Heidelberg secondary structure prediction method.

### 2.11. 3D Structure Modeling of Bg\_9562

The 3D structure of Bg\_9562 is not available in the Protein Data Bank (PDB) (<http://www.rcsb.org/pdb>, accessed on 24 January 2022) Due to the absence of a suitable structural template, homology modeling was not successfully utilized. Thus, using the comparative/homology modeling, web-based servers PHYRE 2.0 (Protein Homology/analogy Recognition Engine), HHpred, RAPTORX, (PS)<sup>2</sup>-v2 and SWISS MODEL generated models with less confidence, and their Verify 3D values and overall quality factor (ERRAT) were not within the accepted range (Table S7).

In order to obtain the high-quality structure of Bg\_9562, ab initio and threading approaches were deployed. By using these approaches, five models were generated through LOMETs (Local Meta-Threading Server), ten models generated through SPARKS, five models from QUARK and five models from Robetta. The models generated through LOMETs and SPARKS did not qualify upon validation using Verify 3D, ERRAT and Ramachandran plot. The most appropriate approach was ab initio using Robetta and QUARK. The models generated by Robetta and QUARK were similar in Verify 3D and ERRAT, while values varied with the evaluation with Ramachandran plot (Table S7). Model four of Robetta displayed allowed values of Z-score (−7.4) and QMEAN4 (−1.42), and Verify 3D (100%) and ERRAT (98.05%) and Ramachandran plot favored regions with 87.4%. We selected this as the best model for the 3D structure of Bg\_9562 (Figure 5C,D). For this predicted 3D structure, the COACH tool (consensus approach to protein–ligand binding site prediction) predicted the binding ligands as nucleic acids and zinc with lower confidence scores of 0.07 C-Score and 0.05 C-Score, respectively. C-Score, as predicted using the COACH tool, defines the confidence score of prediction and it ranges 0–1, where a higher score indicates more reliable prediction. The consensus binding residues of Bg\_9562 for nucleic acids included 38, 67, 78, 90, and 91 and for that of zinc were 82 and 85 residues of Bg\_9562.

AlphaFold 2 also predicted a highly accurate structure of Bg\_9562. The three outputs of AlphaFold 2 are represented in Figure 6. The first output is the 3D coordinates of Bg\_9562 (Figure 6A). The second output is per residue confidence metric, called pLDDT, that corresponds to the model's predicted score on the LDDT-C $\alpha$  metric, which is usually in the range of 0–100. The Local Distance Difference test (LDDT) score is computed using only distances between C $\alpha$  atoms in the protein model. The obtained model for Bg\_9562 was found to be highly accurate, possessing the regions with pLDDT > 90. The third output was Predicted Aligned Error, which is required to assess the confidence in the domain packing and large-scale topology of the protein. The dark green color indicated low error in predicted domains and relative orientations of Bg\_9562 (Figure 6C).

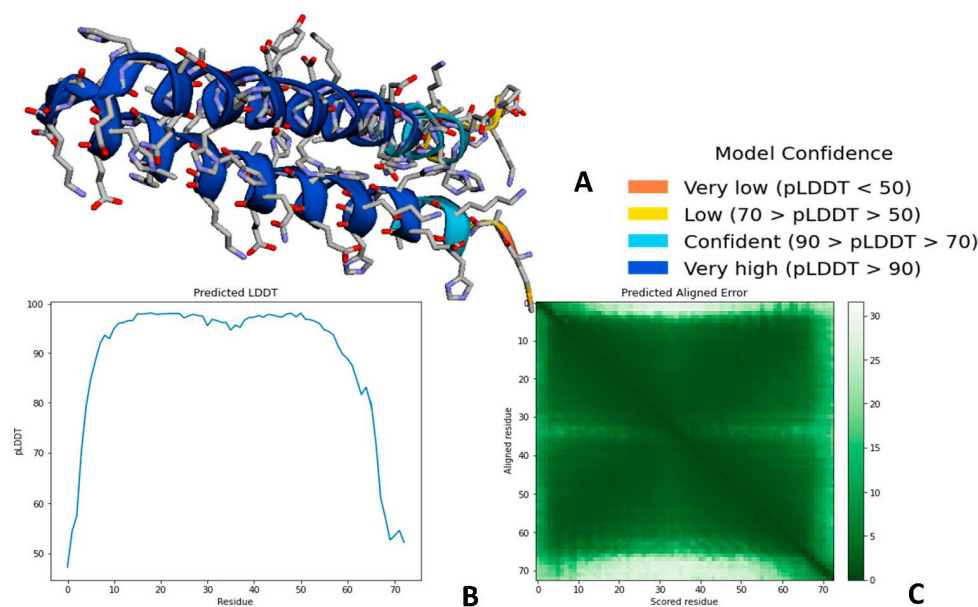


**Figure 6.** The three outputs of AlphaFold v2.1.1.0. online tool. (A) Predicted 3D structure of Bg\_9562 using AlphaFold 2. The predicted model has very high confidence levels of pLDDT > 90. (B) The predicted LDDT (pLDDT) plot gives best information on intra-domain confidence and it interpreted as high as pLDDT > 90. (C) Interactive 2D plot of Predicted Aligned Error (PAE), the dark green color at (x, y) indicated AlphaFold 2 predicted low error with well-defined relative positions from two different domains.

### 2.12. Functional Analysis of Conserved and Disordered Regions of Bg\_9562

The ConSurf server provided results on the characterization of the functional regions. It indicated that the functional regions of Bg\_9562 were highly conserved. The degree of conservation of the amino acid sites among 50 homologs with similar sequences to Bg\_9562 was estimated. The results generated consisted of a structural representation of the protein (Figure S1a), which contains a colorimetric conservation score. Out of 1160 HMMER (homology search algorithm of ConSurf server) generated hits, 1084 were found to be unique and the calculation was performed on the 50 sequences closest to the query i.e., Bg\_9562. The phylogenetic tree was constructed using a phylogeny.fr tool using default parameters and the obtained phylogenetic tree is represented in Figure S1b. The protein sequence was also subjected to motif analysis using MEME Suite 5.4.1 (Multiple Em for Motif Elicitation) and three motifs were predicted to be conserved, which are presented in Table S8. These motifs predicted using MEME were defined as recurring and fixed length patterns in the Bg\_9562 sequence. These motifs were selected based on the lowest *E*-value (Expect value) of prediction. The disordered region of Bg\_9562 was predicted using the PrDOS server (Protein Disorder Prediction System) and the fold index© tool. Both the tools predicted that the N-terminal region (1–14 residues) of Bg\_9562 residues were disordered and the PrDOS tool predicted C-terminal residues (101 to 111) were also disordered (Figure S2a,b).

### 3. Discussion

Invasion of crops by pests and diseases has recently seen a great jump because of several factors, including high intensity and a more input-oriented system of crop cultivation [20]. Further, this increase has warranted the use of more pesticides, leading to several unwanted developments such as health issues of consumers [21] and rejection of export consignments [22]. Eco-friendly management of pests and diseases using microbes and their products has provided an alternative to the use of synthetic plant protection chemicals [23]. The search for novel antifungal agents such as secondary metabolites and antifungal proteins is of considerable interest, especially in the case of certain pathogens

such as RS, where the availability of host plant resistance is not yet available [24]. Bg\_9562 is a novel antifungal protein isolated from the bacteria *B. gladioli* strain NGJ and found to be very effective against RS. However, the efficient use of Bg\_9562 requires a complete understanding of its physiochemical properties for possible effective formulation, identification of molecular targets, and translocation within the plant system. Antimicrobial proteins (AMPs) are currently being considered as a promising alternative for antifungal drugs. However, most of the naturally occurring and synthetically obtained AMPs have so far proven challenging to turn into therapeutic compounds due to concerns about cytotoxicity, low stability, salt sensitivity and a high cost of production. Indeed, several AMPs have displayed significant toxicity for human cell membranes (e.g., pardaxin, melittin and several cathelicidins are cytotoxic due to their membrane lytic mechanism of action [25–27]). In addition, it is well known that physiological salt concentrations can sometimes reduce the effectiveness of cationic AMPs. Therefore, the synthesis of short AMPs containing an appropriate mix of hydrophobic and cationic amino acids with low cytotoxicity and reduced sensitivity to salt is essentially required to design clinically useful AMPs. This strategy is being deployed in many laboratories across the globe [28–30]. In the absence of the crystal structure of Bg\_9562 to date, we have determined its stability, structural and functional properties through wet-lab experiments and in silico computational approaches.

Bg\_9562 was subjected to two different pH and temperature treatments followed by testing their effectivity against RS in vitro. These temperature and pH ranges were determined based on the conditions in which rice is grown in the country (<http://www.knowledgebank.irri.org/rice-knowledge-for-india/india>, accessed on 20 August 2020). Significant bioactivity of the protein at higher temperatures (45 °C) indicates the thermostability of the protein to withstand application in the late sown crop in tropical conditions, where the temperature ranges above 35 °C during most stages of the crop cycle [31]. Positive compatibility studies of Bg\_9562 with native antagonistic/plant growth promoting fungi and bacteria isolated and characterized at this institute, viz., TAIK and BIK3 strains [18], would help in co-application of Bg\_9562 along with the biocontrol agents for the management of ShB disease in rice. In addition to their plant protection properties, plant growth promotion by *Bacillus* and *Trichoderma* species will give an additional benefit to the plants. This combined application would thus increase the efficiency of the management of sheath blight disease, save time and energy for farmers, reduce the cost of production, and increase yield and farmers' incomes.

A study on comparison of the amino acid sequences of the several thermophilic proteins showed that amino acid residues, viz., arginine and tyrosine, were more common, and cysteine and serine were often found in the thermophilic proteins [32]. Interestingly, Bg\_9562 amino acid composition showed only slight similarity to thermophilic protein sequences, with the presence of four arginine residues and only one cysteine residue. Thus, the thermostability of Bg\_9562 may be attributed to the presence of the higher aliphatic amino acids (A, I, L and V), which is similar to reported studies on various thermostable proteins [33].

Protein surface has a net charge depending on the type of amino acids and on the pH. A zero net charge due to the neutralization of charges exists at a specific pH, called the isoelectric point, mostly ranging from pH 5 to 8. Many AMPs retain antimicrobial activity at wide pH ranges. AMPs have enhanced activity at low pH due to their basic properties. This condition is related to the protonation of histidine at acidic pH that promotes electrostatic interactions with anionic surfaces. Bg\_9562 was sensitive to both the pH extremities and was functional at neutral pH. Bg\_9562 was predicted to possess only one histidine residue, which may have resulted in less antifungal activity in low pH conditions in our lab experiments. Bg\_9562 was predicted to possess an isoelectric pI of 4.65 and net charge of  $-3.75$  at neutral pH. The effect of pH on the antibacterial activity of AMPs varies, for example, thanatin activity at neutral pH is slightly higher than that under acidic conditions. By contrast, the activity of xylan on *E. coli*, *Listeria*, and *C. albicans* is remarkably higher at pH 5.5 than at pH 7.4 [34]. A charge at the surface enables the protein to interact

with water and a zero charge protein interacts with other proteins and precipitates [35]. A class III haem peroxidase protein from leaves of *Acorus calamus*, with a molecular weight of 32 kDa, pI of 7.93, maximum activity at pH 5.5, temperature stability from 5 °C to 60 °C and optimum at 36 °C, was found to inhibit the pathogenic fungi *Fusarium moniliforme* from rice and *Macrophomina phaseolina* from black gram [36].

AMPs are generally distinguished by variations in their length, amino acid sequence and structural properties (helical, beta-sheet, turns, extended, etc.) [37–39]. The sequence length of Bg\_9562 was found to be 111 amino acids, which is consistent with the property of antimicrobial peptides. Most of the AMPs are characterized by a short peptide length and generally consist of 12–100 amino acid residues [40]. This minimizes the probability of being degraded by bacterial proteases. In general, most of the AMPs are highly cationic, consisting of lysine (Lys) and/or arginine (Arg) residues and 50% hydrophobic amino acids. The Bg\_9562 protein contains 46 hydrophobic amino acids (41%) with the maximum presence of alanine residues (14.4%). The aromatic amino acids, tyrosine and tryptophan, are completely absent and two phenylalanine residues are present in Bg\_9562. In general, the presence of large aromatic residues in proteins prefers T-shaped interactions which influence the protein structure to a large extent. Individual interactions between these residues provide little stability to the structure, while the cumulative effect of their interactions contributes significantly to the conformational stability of the overall protein structure [41]. The phenylalanines have the tendency to pair with themselves—Phe–Phe pairs [42]. Tyrosine residues, on the other hand, tend to bind more with DNA and RNA and are more involved in the DNA–protein complexes [43]. The absence of tyrosine and tryptophan amino acids in the sequence of Bg\_9562 might result in less affinity to be intact and might allow Bg\_9562 to interact more with the sugars in the cell walls of RS. Aromatic amino acids once metabolized behave as precursors for a variety of substances in the cell [44]; however, with the absence of such aromatic amino acid residues Bg\_9562 may not be able to be a precursor for the synthesis of other active compounds and may be a simple protein produced at the tail end of the metabolic pathway that is involved in the defense of the bacteria that produce it. The assessment of the secondary structure of Bg\_9562 showed the presence of more random coils than the alpha helix. Random coils are one of the non-native states of proteins [45]. Non-native states of proteins are of increasing research interest because of their relevance to protein folding, translocation, and stability [46]. The 3D structure of proteins can be modeled via the comparative method (both comparative modeling and threading), which depends on known protein structures, or by ab initio, which relies on amino acid sequences. To date, comparative modeling is the most successful and accurate method, as evolutionarily related proteins usually share a similar structure (sequence identity > 30%). However, searching for homologous proteins is relatively difficult when the sequence identity is low or known as the “twilight zone”, where the sequence identity falls between 10–30%. When confronted with this problem, threading or ab initio are alternate methods to obtain the protein structure. As Bg\_9562 was also categorized into the twilight zone with less sequence identity to known proteins, ab initio method-based tools were deployed, and an appropriate validated 3D model was developed using Robetta.

Most AMPs share amphipathic properties, which allow the cationic peptides to bind to negatively charged microbial membrane surfaces. In general, most of the antimicrobial peptides have a positive net charge (mostly between +2 to +4) at pH 7, which provides binding specificity to the negatively charged bacterial membranes through electrostatic interactions [47], and less than 5% of AMPs have a net negative charge. In addition, these peptides mostly have an isoelectric point close to 10 [48], which is very similar to soap or detergent. The anionic AMPs (those possessing net negative charge) have a large number of negatively charged aspartic and glutamic acid residues [49]. The net charge of Bg\_9562 was predicted as −3.75 and isoelectric pI was calculated as 4.65. Bg\_9562 was classified as an anionic AMP with 12 negatively charged residues (aspartic acid + glutamic acid). Anionic AMPs require zinc as a functional co-factor and the zinc complex shows stronger

antibacterial activity [50]. Several of these AMPs use metal ions to form cationic salt bridges with the negatively charged components of the microbial membrane to penetrate the membrane. Anionic AMPs attach to the ribosomes or inhibit ribonuclease activity when in the cytoplasm [51]. Interestingly, zinc was also predicted as a ligand by the COACH server with a lower confidence score of 0.05 for the developed 3D model of Bg\_9562. Thus, we predict that Bg\_9562 may interact with zinc ions for its efficient penetration into fungal membrane. Nevertheless, further experiments are required to confirm its mode of action.

Another vital property of AMPs is hydrophobicity. Creating pores in the cytoplasmic membrane of the fungal cell requires hydrophobic residues that interact with the lipid bilayer, i.e., the hydrophobic portion [52]. This interaction results in the degradation of the cytoplasmic membrane. Low hydrophobicity may be insufficient to induce an effective interaction between these peptides and cytoplasmic membranes, which decreases antimicrobial activity. Nevertheless, the exceptionally high hydrophobicity of AMPs leads to their auto-association and inability to penetrate/enter the membranes [52]. The Bg\_9562 protein documented optimal hydrophobicity of 41%, which aids in efficient interaction with fungal membranes. Interestingly, a transmembrane region from 83 to 102 amino acid residues of Bg\_9562 was predicted which contributes to efficient interaction with cell membranes. The positive Boman index of Bg\_9562 predicted as 1.27 kcal/mol also enhances the ability of Bg\_9562 to bind to cell membrane proteins. The Boman index is essentially the average hydrophobic value measured using the Radzicka–Wolfenden scale [53]. The GRAVY index of Bg\_9562 was slightly negative (−0.012), meaning that the protein is hydrophilic in nature. This is a paradox and needs to be reinvestigated. Protein solubility is variable and is affected by the number of polar and non-polar groups and their arrangement along the molecule. Generally, proteins are soluble only in strong polar solvents such as water, glycerol or formic acid, and rarely soluble in less polar solvents such as ethanol. The hydrophilic nature of Bg\_9562 may indicate its high solubility in solutions. The interaction between hydrophobic groups is reported to be the most important force that maintains the tertiary structure of proteins [54]. The negative GRAVY may indicate that the tertiary structure of Bg\_9562 may be less stable, leading to a flexible action upon reaching the target. However, the half-life period of Bg\_9562 is very long (30 h), indicating a long persistent protein when compared to other proteins which have a half-life period ranging less than 10 h [55]. In the present study, the structure analysis of Bg\_9562 indicated that it does not possess lytic domains and thus may not be toxic. In addition, Bg\_9562 is reported to possess a phage tail Gp41 domain [17]. Several studies reported the use of tail proteins as novel antimicrobial peptides [56]. A novel phage tail-like bacteriocin, designated maltocin P28, was extracted from *Stentrophomonas maltophilia* and found to possess strong bactericidal activity against 38 of 81 tested *S. maltophilia* strains [57]. Similarly, the tail protein named R-type syringacin, from *Pseudomonas syringae*, was found to be highly conserved and lethal to other strains of *Pseudomonas* [58]. Interestingly, the structure prediction analysis for the intrinsically folded or disordered region in Bg\_9562 sequences revealed that the N-terminal region is intrinsically disordered. Similarly, the PrDOS server estimated that both N-terminal (1–14 residues) and C-terminal (101–111 residues) regions of Bg\_9562 were in disorder, while the fold index© tool indicated only the N-terminal region (1–26 residues) of Bg\_9562 was disordered. The proteins that are in intrinsic disorder usually serve in the cell signaling functions and regulation. The disorder blocks in IDPs allow the simultaneous interaction with many proteins, and therefore, proteins act as multifunctional proteins in physiological conditions [59,60]. Thus, due to the presence of IDPs, Bg\_9562 might be able to cope in the different physiological salt concentrations, retaining its functional ability even at higher pH concentrations. In addition, ProtParam tool analysis predicted Bg\_9562 to be a stable protein with the instability index value of 21.19 and estimated half-life of >20 h, indicating the potential of Bg\_9562 in enduring the process of development of different formulations, including encapsulations to be effective against sheath blight disease.

Many bacterial proteins are tethered to the inner or outer membranes via long acyl chains. These lipid anchors are covalently attached to specific N-terminal cysteines of

periplasmic proteins as they emerge from the Sec machinery, forming lipoproteins, and can then be inserted into the appropriate membrane [61]. The highly hydrophobic tails of lipoproteins prevent them from crossing the periplasmic space alone, and a specialized localization of the lipoprotein (Lol) pathway is used to sort and traffic those destined for the outer membrane [61]. The PSORT tool predicted that Bg\_9562 is more likely to target the nucleus of the RS, with a probability of 47.8%. Interestingly, nucleic acids present in the nucleus were predicted as ligands using the COACH server for the modeled tertiary structure of Bg\_9562 with a confidence score of 0.07. It may thus be hypothesized that the mode of action of Bg\_9562 is through regulation of transcription by binding to specific regions that bind to nucleic acids in *R. solani*, but further experimentations are required to confirm this hypothesis. Recent studies by [62] confirmed a similar result where a synthetic KW<sub>4</sub> antifungal protein against *C. albicans* could inhibit cellular functions by binding to RNA and DNA after it has been translocated into cells, resulting in the eradication of *C. albicans*. In the same study the authors conducted several studies including fluorescence spectroscopy, scanning electron microscopy, laser-scanning confocal microscopy and gel retardation assays to confirm the mode of action of the antifungal KW<sub>4</sub> protein as estimated by the in silico analysis.

#### 4. Materials and Methods

##### 4.1. Preparation of Pure Bg\_9562 Protein

The pure form of protein Bg\_9562 was obtained from National Institute of Plant Genome Research laboratory (NIPGR, Delhi, India). The laboratory procedure for protein expression and purification was described in [17]. After confirming the presence of ~13 kD band in Western blot, the purified protein Bg\_9562 was utilized for all further experiments.

##### 4.2. Broad-Spectrum Bioactivity Assay of Bg\_9562 on Fungal and Bacterial Growth

Individual axenic cultures of RS, TAIK1 and BIK3 were grown on Potato Dextrose Agar (PDA) and Luria Broth Agar (LBA) media, respectively, and kept for incubation at room temperature. Using a cork borer, mycelial discs were collected and were dipped in 1 mL (100 µg/mL) of protein and incubated at two temperatures, viz., 35 °C, 45 °C; pH 3.0, 9.5 ( $n = 3$ ) and at time intervals, viz., 6, 12 and 24 h along with positive (purified Bg\_9562 protein at standard temperature and neutral pH) and negative controls (axenic cultures of RS, TAIK1, BIK3). After treatment, fungal/bacterial discs were washed individually in sterile distilled water and placed on fresh PDA and LBA plates and were incubated at their respective growth temperatures. Observations in the form of mycelial growth or bacterial colonies were observed after 6, 12 and 24 h in terms of mycelial lawn area (RS, TAIK1) and bacterial colonies (BIK3) observed in treated and control plates. The experiment was repeated three times.

##### 4.3. Efficacy of Bg\_9562 Protein under Field Conditions

To test the efficacy of Bg\_9562 protein, pilot field trials were taken up in a rice variety TN1. The field trials were laid out in a Randomized Block Design with three replications and three treatments (pre-infection, post-infection and co-inoculation of RS and protein) against rice sheath blight disease at varying concentrations of the protein, viz., 2.5 ppm, 5.0 ppm, 7.5 ppm and 10 ppm, and with a spray volume of 833 mL/T maintaining positive (Carbendazim 50% WP) and negative (untreated) controls (Table S9).

##### 4.4. Sequence Retrieval

Nucleotide sequence of the Bg\_9562 gene of *B. gladioli* strain NGJ1 was retrieved from the NCBI database using accession code KX620741. It was then translated to polypeptide sequence using the online tool ExPASy-translate [63] and it was used for further in silico analysis in the study. The computational approaches utilized in every step of the in silico study are described briefly as a flowchart (Figure S3). Various online software/servers

deployed at each step in the *in silico* analysis are listed and their URL details are given in Table S4.

#### 4.5. Prediction of Physicochemical Properties of Bg\_9562 Protein

The amino acid composition and various other physicochemical properties of Bg\_9562, including theoretical pI, molecular weight, bulkiness, polarity, aliphatic index and instability index were estimated using the online tools ExPasy-ProtParam [63] and ProtScale [63] that are available for free use in the public domain. The hydrophobicity plot of the contiguous amino acid residues of Bg\_9562 was determined by constructing the Kyte–Doolittle hydrophathy graph [64]. Other parameters, i.e., Wimley–White whole-residue hydrophobicity of the peptide, protein binding potential (Boman index) and antimicrobial potential were calculated using predictive online tools of the Antimicrobial Peptide Database v.2.34 (APD2; <http://aps.unmc.edu/AP/main.php>, accessed on 31 August 2020) [65]. The Boman index is an estimate of protein-binding potential, calculated on the basis of cyclohexane-to-water partition coefficient of the respective amino acid side chains divided by the total number of amino acid residues within the peptide [19]. Wimley–White whole-residue hydrophobicity of the peptide (the sum of whole-residue free energy of transfer of peptide from water to phosphatidylcholine interface) calculates the protein hydrophobicity, and the higher its value the more likely the protein is to be hydrophobic [66].

#### 4.6. Prediction of Functional Properties of Bg\_9562 Protein

The motifs in the Bg\_9562 protein were predicted using the default parameters in the MEME Suite 5.4.1 (Multiple Em for Motif Elicitation) [67]. MEME represents motifs as position-dependent letter–probability matrices that describe the probability of each possible letter at each position in the pattern. The prediction of transmembrane-spanning regions and their orientation in the protein Bg\_9562 was performed using TMPred online software. The algorithm is based on the statistical analysis of TMbase, a database of naturally occurring transmembrane proteins [68]. Another tool that predicts topology of membrane proteins is based on a hidden Markov model; TMHMM-2.0 server was employed [69]. The property of localization of Bg\_9562 within the cells was predicted using the PSORT program [70].

Online database CRYSTALP2 [71] was used to predict the propensity of the protein to crystallize. Either fully or partially disordered proteins have little tendency to crystallize. The sequence-based prediction of the propensity for production of diffraction-quality crystals, production of crystals, purification and production of the protein material was predicted using the online database PPCpred [72]. A ConSurf server was employed to identify the conserved and biologically important residues in the amino acid sequences of Bg\_9562 [73]. The degree to which an amino acid position is evolutionarily conserved (i.e., its evolutionary rate) is strongly dependent on its structural and functional importance. Thus, conservation analysis of positions among members from the same family can often reveal the importance of each position protein structure or function. In ConSurf, evolutionary rate is estimated based on the evolutionary relatedness between the protein and its homologues and considering the similarity between amino acids as reflected in the substitution matrix methods. The multiple alignment was built using MAFT and UNIREF90 was used for the collection of homologs using HMMER homology search algorithm of the ConSurf database. These generated sequences that were closest to the given query, i.e., Bg\_9562 were selected for phylogenetic tree representation. The phylogenetic tree was constructed using Pylogeny.fr, an online database tool [74].

#### 4.7. Secondary Structure Prediction

The secondary structure of Bg\_9562 protein was predicted using PSIPRED 4.0 workbench [75] and in addition, the secondary structure of the protein was also predicted employing NPS@ server. The Network Protein Sequence @analysis (NPS@) is an interactive webserver dedicated to protein sequence analysis [76]. Secondary structure prediction us-

ing NPS@ server was performed with various methods, viz., DSC [77], HNN [78], PHD [79], PREDATOR [80], MLRC [81] SIMPA96 [82] and secondary consensus [83] keeping default parameters for 4 state predictions and keeping output width = 70.

#### 4.8. 3D Structure Prediction

To obtain a high-quality model of Bg\_9562 protein, its tertiary structure was modeled using in silico methods including homology modeling, threading and ab initio. For comparative homology modeling, web-based server HHPred [84] was used and the best alignment suggested by HHPred that is typically collected using the PSIBLAST program was used. The atomic coordinates built on this target template alignment were generated using MODELLER v. 9.2 [85]. Another web-based server, Phyre2, was used, which uses the hidden Markov method to generate alignments of a submitted protein sequence against proteins with published structures [86]. The resulting alignments were then used to produce homology-based models of the query sequence to predict its three-dimensional structure. RaptorX uses a non-linear scoring function to combine homologous information with structural information for a given template–sequence alignment. It uses NEFF to adjust the relative importance of homology and structural information. RaptorX uses a combination of RaptorX-Boost and Raptor-X MSA to build 3D models for a target–template alignment [87]. SWISS MODEL was used for predicting and analyzing homology-based 3D protein structure [88]. Web-based threading servers, LOMETS (which builds 3D models by collecting high-scoring target-to-template alignments from locally installed threading programs FFAS3D, HHsearch, MUSTER, pGenTHREADER, PPAS, PRC, PROSPECT2, SP3 and SPARKS-X) [89] and I-TASSER that generates 3D models based on the hierarchical method for protein structure and function prediction were employed [90]. Further, SPARKSX, that constructs 3D models based on the application of probabilistic-based matching between predicted primary structural properties of the query and corresponding native properties of templates was also used in the study [91]. For proteins such as Bg\_9562, which has very little homology with known templates, another method, ab initio, was deployed. Ab initio is a de novo protein structure prediction that builds 3D models of proteins from primary structures in the presence or absence of homologs to the given query protein. Robetta by Baker’s lab, whose protein structure prediction is continuously evaluated using CAMEO, was deployed for ab initio method [92] and another tool was QUARK [93]. As the existing methods fall far short of atomic accuracy, especially when no homologous template is available, another most powerful tool based on neural network-based model, AlphaFold 2 [94], was utilized to build highly accurate model of Bg\_9562.

AlphaFold 2 on Google Colab’s Notebook [95] was used to model Bg\_9562. This Colab notebook allows easy prediction of protein using a slightly simplified version of AlphaFold v.2.1.0. Colab notebooks are coupled to a special sequence search program, MMSeqs2, thus making this technology more powerful.

#### 4.9. 3D Structure Validation

The 3D structure validation of modeled protein was carried out by PROSA, QMEAN4 and Ramachandran webservers. Using PROCHECK [96] plot to visualize backbone torsional angles,  $\psi$  and  $\phi$  of residues in protein structures were drawn. It is a universal way to calculate the number of residues in favored, allowed and outlier regions in the given protein. PROSA webserver is a frequently employed tool in the validation of protein structures obtained from X-ray analysis, NMR spectroscopy and theoretical calculations. QMEAN4 is a linear combination of four statistical potential terms. It predicts a global IDDT score in the range (0,1) and the value calculated by the webserver is transformed into a Z-score [97]. After selecting the best evaluated 3D structure of Bg\_9562, ligands binding to it were predicted using the COACH server [98]. COACH is consensus approach to protein–ligand binding site prediction. When the given structure is subjected to COACH server, it predicts complementary ligand binding sites using combined multiple prediction results of algorithms from TM-SITE, S-SITE, COFACTOR, and FINDSITE [98].

#### 4.10. Prediction of Disordered Regions in Bg\_9562

The disordered regions in the protein have immense importance in governing the structure and function of a protein. Disordered regions of Bg\_9562 were identified using Protein Disorder Prediction System (PrDOS) server [99]. PrDOS predicts natively disordered regions of protein from its amino acid sequence and returns the disordered probability of each residue as prediction result. The default parameters with 5% false positive rate were used while executing the disordered regions of Bg\_9562. Another simple versatile tool, fold index<sup>©</sup>, was deployed for estimating the disordered regions in Bg\_9562. Fold index<sup>©</sup> predicts if the given protein intrinsically unfolded by implementing the algorithm of Uversky and co-workers based on the average residue hydrophobicity and net charge of the sequence [100].

## 5. Conclusions

The current study of the in silico analysis of physicochemical properties coupled with wet-lab experiments of Bg\_9562 help in better understanding of the protein and its functional characterization, further facilitating in the identification of fungal–protein interactions and membrane and nucleic acid interactions associated with the broad-spectrum antifungal activity of the protein. Furthermore, considering its broad-spectrum antifungal activity, the protein may be potentially useful in biotechnological applications to control fungal diseases. According to our results, Bg\_9562 is a stable protein with a single trans-membrane region, possesses the right amount of aliphatic index and hydropathicity index values, and is essentially nontoxic to be used as an antifungal drug. In short, bioinformatics analysis would be helpful to choose the functional and targeted segments of the protein for preparations of specific formulations for controlling sheath blight disease of rice.

**Supplementary Materials:** The following supporting information can be downloaded at: <https://www.mdpi.com/article/10.3390/antibiotics11030363/s1>, Figure S1: Functional properties of Bg\_9562 predicted using Consurf server. Figure S2: Prediction of disordered region of Bg\_9562 using PrDOS and fold index<sup>©</sup> tools. Figure S3: Flow diagram describing the in silico tools used in the study. Table S1: Effect of Bg\_9562 protein on *R.solani* mycelial growth. Table S2: Protein efficiency check under field conditions during foliar treatment in cultivar TN1. Table S3: Amino acid sequence of Bg\_9562 protein. Table S4: List of online tools and their URLs utilized in the study. Table S5: Amino acid composition of Bg\_9562 protein. Table S6: Minimum and maximum values of physicochemical properties of Bg\_9562 protein predicted using ProtScale. Table S7: Models of Bg\_9562 calculated by various methods/servers and their validation results. Table S8: Motifs predicted in Bg\_9562 using MEME software. Table S9: Evaluation of efficacy of Bg\_9562 protein molecule against sheath blight of rice (*Cv.* TN-1) under field conditions.

**Author Contributions:** Conceptualization and methodology: K.C., R.M.S., P.K., R.G., K.M.B., G.J. and V.P.; formal analysis, methodology and software: P.K., R.G., D.M. and K.M.B.; investigation and validation: P.K., R.G., D.M., P.C., M.P. and H.S.; original draft writing: P.K., K.C. and R.G.; review and editing manuscript: P.K., D.M., K.M.B., R.M.S. and G.J. All authors have read and agreed to the published version of the manuscript.

**Funding:** The authors wish to acknowledge the funding received from the Department of Biotechnology, Government of India through its research project grant no. (102/IFD/SAN/765/2019-20).

**Institutional Review Board Statement:** Not applicable.

**Informed Consent Statement:** Not applicable.

**Data Availability Statement:** Not applicable.

**Acknowledgments:** The authors would also like to thank the Indian Council of Agricultural Research and Department of Biotechnology, Government of India, for the generous funding support for the research work presented in the study.

**Conflicts of Interest:** The authors declare no conflict of interest.

## References

1. Den Herder, G.; Van Isterdael, G.; Beeckman, T.; De Smet, I. The roots of a new green revolution. *Trends Plant Sci.* **2010**, *15*, 600–607. [CrossRef] [PubMed]
2. Thambugala, K.M.; Daranagama, D.A.; Phillips, A.J.; Kannangara, S.D.; Promputtha, I. Fungi vs. fungi in biocontrol: An overview of fungal antagonists applied against fungal plant pathogens. *Front. Cell. Infect. Microbiol.* **2020**, *10*, 718. [CrossRef] [PubMed]
3. Jangir, M.; Sharma, S.; Sharma, S. Development of next-generation formulation against *Fusarium oxysporum* and unraveling bioactive antifungal metabolites of biocontrol agents. *Sci. Rep.* **2021**, *11*, 22895. [CrossRef] [PubMed]
4. Huan, Y.; Kong, Q.; Mou, H.; Yi, H. Antimicrobial Peptides: Classification, Design, Application and Research Progress in Multiple Fields. *Front. Microbiol.* **2020**, *11*, 582779. [CrossRef] [PubMed]
5. Shai, Y. Molecular recognition between membrane-spanning polypeptides. *Trends Biochem. Sci.* **1995**, *20*, 460–464. [CrossRef]
6. Balkovec, J. Lipopeptide antifungal agents. *Expert Opin. Investig. Drugs* **1994**, *3*, 65–82. [CrossRef]
7. Debono, M.; Gordee, R.S. Antibiotics that inhibit fungal cell wall development. *Annu. Rev. Microbiol.* **1994**, *48*, 471–497. [CrossRef]
8. Singh, H.B. Management of plant pathogens with microorganisms. *Proc. Indian Natl. Sci. Acad.* **2014**, *80*, 443–454. [CrossRef]
9. World Rice Production 2019/2020 World Agricultural Production. Available online: <http://www.worldagriculturalproduction.com/crops/rice.aspx> (accessed on 11 April 2020).
10. Gao, J.P.; Chao, D.Y.; Lin, H.X. Understanding abiotic stress tolerance mechanisms, recent studies on stress response in rice. *J. Integr. Plant Biol.* **2007**, *49*, 742–750. [CrossRef]
11. Gangopadhyay, S.; Chakrabarti, N.K. Sheath blight of rice. *Rev. Plant Pathol.* **1982**, *61*, 451–460.
12. Carling, D.; Baird, R.; Gitaitis, R.; Brainard, K.; Kuninaga, S. Characterization of AG-13, a newly reported anastomosis group of *Rhizoctonia solani*. *Phytopathology* **2002**, *92*, 893–899. [CrossRef] [PubMed]
13. Carling, D.; Kuninaga, S.; Brainard, K. Hyphal anastomosis reactions, rDNA-internal transcribed spacer sequences, and virulence levels among subsets of *Rhizoctonia solani* anastomosis group-2 (AG-2) and AG-BI. *Phytopathology* **2002**, *92*, 43–50. [CrossRef] [PubMed]
14. Singh, P.; Mazumdar, P.; Harikrishna, J.A.; Babu, S. Sheath blight of rice: A review and identification of priorities for future research. *Planta* **2019**, *250*, 1387–1407. [CrossRef] [PubMed]
15. Berlin, A.; Källström, H.N.; Lindgren, A.; Olson, Å. Scientific evidence for sustainable plant disease protection strategies for the main arable crops in Sweden. A systematic map protocol. *Environ. Evid.* **2018**, *7*, 31. [CrossRef]
16. Köhl, J.; Kolnaar, R.; Ravensberg, W.J. Mode of action of microbial biological control agents against plant diseases: Relevance beyond efficacy. *Front. Plant Sci.* **2019**, *10*, 845. [CrossRef]
17. Swain, D.M.; Yadav, S.K.; Tyagi, I.; Kumar, R.; Kumar, R.; Ghosh, S.; Das, J.; Jha, G. A prophage tail-like protein is deployed by *Burkholderia* bacteria to feed on fungi. *Nat. Commun.* **2017**, *8*, 404. [CrossRef]
18. Kannan, C.; Mishra, D.; Rekha, G.; Maruthi, P.; Shaik, H.; Sundaram, R.M. Diversity analysis of antagonistic microbes against bacterial leaf and fungal sheathblight diseases of rice. *Egypt. J. Biol. Pest Control* **2021**, *31*, 115. [CrossRef]
19. Boman, H.G. Antibacterial peptides: Basic facts and emerging concepts. *J. Intern. Med.* **2003**, *254*, 197–215. [CrossRef]
20. Molla, K.A.; Karmakar, S.; Molla, J.; Bajaj, P.; Varshney, R.K.; Datta, S.K.; Datta, K. Understanding sheath blight resistance in rice: The road behind and the road ahead. *Plant Biotechnol. J.* **2020**, *18*, 895–915. [CrossRef]
21. Khammanee, N.; Qiu, Y.; Kungskulniti, N.; Bignert, A.; Meng, Y.; Zhu, Z.; Teffera, Z.L. Presence and Health Risks of Obsolete and Emerging Pesticides in Paddy Rice and Soil from Thailand and China. *Int. J. Environ. Res. Public Health* **2020**, *17*, 3786. [CrossRef]
22. Chatterjee, S.; Gangopadhyay, C.; Bandyopadhyay, P.; Bhowmick, M.; Roy, S.; Majumder, A.; Gathala, M.; Tanwar, R.; Singh, S.; Birah, A.; et al. Input-based assessment on integrated pest management for transplanted rice (*Oryza sativa*) in India. *Crop Prot.* **2021**, *141*, 105444. [CrossRef]
23. Selitrennikoff, C.P. Antifungal proteins. *Appl. Environ. Microbiol.* **2001**, *67*, 2883–2894. [CrossRef] [PubMed]
24. Dey, S.; Badri, J.; Prakasam, V.; Bhadana, V.P.; Eswari, K.B.; Laha, G.S.; Priyanka, C.; Aku, R.; Ram, T. Identification and agro-morphological characterization of rice genotypes resistant to sheath blight. *Australas. Plant Pathol.* **2016**, *45*, 145–153. [CrossRef]
25. Shai, Y.; Fox, J.; Caratsch, C.; Shih, Y.L.; Edwards, C.; Lazarovici, P. Sequencing and synthesis of pardaxin, a polypeptide from the Red Sea Moses sole with ionophore activity. *FEBS Lett.* **1988**, *242*, 161–166. [CrossRef]
26. Oren, Z.; Hong, J.; Shai, Y. A repertoire of novel antibacterial diastereomeric peptides with selective cytolytic activity. *J. Biol. Chem.* **1997**, *272*, 14643–14649. [CrossRef]
27. Johansson, J.; Gudmundsson, G.H.; Rottenberg, M.E.; Berndt, K.D.; Agerberth, B. Conformation-dependent antibacterial activity of the naturally occurring human peptide LL-37. *J. Biol. Chem.* **1988**, *273*, 3718–3724. [CrossRef]
28. Jin, L.; Bai, X.; Luan, N.; Yao, H.; Zhang, Z.; Liu, W.; Chen, Y.; Yan, X.; Rong, M.; Lai, R.; et al. A Designed Tryptophan- and Lysine/Arginine-Rich Antimicrobial Peptide with Therapeutic Potential for Clinical Antibiotic-Resistant *Candida albicans* Vaginitis. *J. Med. Chem.* **2016**, *59*, 1791–1799. [CrossRef]
29. Godballe, T.; Mojsoska, B.; Nielsen, H.M.; Jenssen, H. Antimicrobial activity of GN peptides and their mode of action. *Biopolymers* **2016**, *106*, 172–183. [CrossRef]
30. Deslouches, B.; Hasek, M.L.; Craigo, J.K.; Steckbeck, J.D.; Montelaro, R.C. Comparative functional properties of engineered cationic antimicrobial peptides consisting exclusively of tryptophan and either lysine or arginine. *J. Med. Microbiol.* **2016**, *65*, 554–565. [CrossRef]

31. Hussain, S.; Khaliq, A.; Ali, B.; Hussain, H.A.; Qadir, T.; Hussain, S. Temperature Extremes: Impact on Rice Growth and Development. In *Plant Abiotic Stress Tolerance*; Hasanuzzaman, M., Hakeem, K., Nahar, K., Alharby, H., Eds.; Springer: Cham, Switzerland, 2019. [\[CrossRef\]](#)
32. Kumar, S.; Tsai, C.J.; Nussinov, R. Factors enhancing protein thermostability. *Protein Eng.* **2000**, *13*, 179–191. [\[CrossRef\]](#)
33. Haki, G.D.; Rakshit, S.K. Developments in industrially important thermostable enzymes: A review. *Bioresour. Technol.* **2003**, *89*, 17–34. [\[CrossRef\]](#)
34. Holdbrook, D.A.; Singh, S.; Choong, Y.K.; Petrlova, J.; Malmsten, M.; Bond, P.J.; Verma, N.K.; Schmidtchen, A.; Saravanan, R. Influence of pH on the activity of thrombin-derived antimicrobial peptides. *Biochim. Biophys. Acta Biomembr.* **2018**, *1860*, 2374–2384. [\[CrossRef\]](#) [\[PubMed\]](#)
35. Mao, A.H.; Crick, S.L.; Vitalis, A.; Chicoine, C.L.; Pappu, R.V. Net charge per residue modulates conformational ensembles of intrinsically disordered proteins. *Proc. Natl. Acad. Sci. USA* **2010**, *107*, 8183–8188. [\[CrossRef\]](#) [\[PubMed\]](#)
36. Ghosh, M. Antifungal properties of haem peroxidase from *Acorus calamus*. *Ann. Bot.* **2006**, *98*, 1145–1153. [\[CrossRef\]](#)
37. Nguyen, L.T.; Haney, E.F.; Vogel, H.J. The expanding scope of antimicrobial peptide structures and their modes of action. *Trends Biotechnol.* **2011**, *29*, 464–472. [\[CrossRef\]](#)
38. Hancock, R.E. Peptide antibiotics. *Lancet* **1997**, *349*, 418–422. [\[CrossRef\]](#)
39. Hwang, P.M.; Vogel, H.J. Structure-function relationships of antimicrobial peptides. *Biochem. Cell Biol.* **1988**, *76*, 235–246. [\[CrossRef\]](#)
40. Kim, H.; Jang, J.H.; Kim, S.C.; Cho, J.H. De novo generation of short antimicrobial peptides with enhanced stability and cell specificity. *J. Antimicrob. Chemother.* **2014**, *69*, 121–132. [\[CrossRef\]](#)
41. Anjana, R.; Vaishnavi, M.K.; Sherlin, D.; Kumar, S.P.; Naveen, K.; Kanth, P.S.; Sekar, K. Aromatic-aromatic interactions in structures of proteins and protein-DNA complexes: A study based on orientation and distance. *Bioinformatics* **2012**, *8*, 1220–1224. [\[CrossRef\]](#)
42. Butterfield, S.M.; Patel, P.R.; Waters, M.L. Contribution of aromatic interactions to alpha-helix stability. *J. Am. Chem. Soc.* **2002**, *124*, 9751–9755. [\[CrossRef\]](#)
43. Meyer, E.A.; Castellano, R.K.; Diederich, F. Interactions with aromatic rings in chemical and biological recognition. *Angew. Chem.* **2003**, *42*, 1210–1250. [\[CrossRef\]](#) [\[PubMed\]](#)
44. Han, Q.; Phillips, R.S.; Li, J. Editorial: Aromatic Amino Acid Metabolism. *Front. Mol. Biosci.* **2012**, *6*, 22. [\[CrossRef\]](#) [\[PubMed\]](#)
45. Smith, L.J.; Fiebig, K.M.; Schwalbe, H.; Dobson, C.M. The concept of a random coil. Residual structure in peptides and denatured proteins. *Fold. Des.* **1996**, *1*, R95–R106. [\[CrossRef\]](#)
46. González-Faune, P.; Sánchez-Arévalo, I.; Sarkar, S.; Majhi, K.; Bandopadhyay, R.; Cabrera-Barjas, G.; Gómez, A.; Banerjee, A. Computational Study on Temperature Driven Structure–Function Relationship of Polysaccharide Producing Bacterial Glycosyl Transferase Enzyme. *Polymers* **2021**, *13*, 1771. [\[CrossRef\]](#)
47. Yeaman, M.R.; Yount, N.Y. Mechanisms of antimicrobial peptide action and resistance. *Pharmacol. Rev.* **2003**, *55*, 27–55. [\[CrossRef\]](#)
48. Torrent, M.; Andreu, D.; Nogués, V.M.; Boix, E. Connecting peptide physicochemical and antimicrobial properties by a rational prediction model. *PLoS ONE* **2011**, *6*, e16968. [\[CrossRef\]](#)
49. Narayana, J.L.; Chen, J.Y. Antimicrobial peptides: Possible anti-infective agents. *Peptides* **2015**, *72*, 88–94. [\[CrossRef\]](#)
50. Jiang, L.; Wang, B.; Li, B.; Wang, C.; Luo, Y. Preparation and identification of peptides and their zinc complexes with antimicrobial activities from silver carp (*Hypophthalmichthys molitrix*) protein hydrolysates. *Food Res. Int.* **2014**, *64*, 91–98. [\[CrossRef\]](#)
51. Jezowska-Bojczuk, M.; Stokowa-Softys, K. Peptides having antimicrobial activity and their complexes with transition metal ions. *Eur. J. Med. Chem.* **2018**, *143*, 997–1009. [\[CrossRef\]](#)
52. Chen, Y.; Guarnieri, M.T.; Vasil, A.I.; Vasil, M.L.; Mant, C.T.; Hodges, R.S. Role of peptide hydrophobicity in the mechanism of action of  $\alpha$ -helical antimicrobial peptides. *Antimicrob. Agents Chemother.* **2007**, *51*, 1398–1406. [\[CrossRef\]](#)
53. Radzicka, A.; Wolfenden, R. Comparing the polarities of the amino acids: Side-chain distribution coefficients between the vapor phase, cyclohexane, 1-octanol, and neutral aqueous solution. *Biochemistry* **1988**, *27*, 1664–1670. [\[CrossRef\]](#)
54. Jiang, Z.Y.; Xu, L.L.; Lu, M.C.; Chen, Z.Y.; Yuan, Z.W.; Xu, X.L.; Guo, X.K.; Zhang, X.J.; Sun, H.P.; You, Q.D. Structure-Activity and Structure-Property Relationship and Exploratory in Vivo Evaluation of the Nanomolar Keap1-Nrf2 Protein-Protein Interaction Inhibitor. *J. Med. Chem.* **2015**, *58*, 6410–6421. [\[CrossRef\]](#) [\[PubMed\]](#)
55. Chen, W.; Smeekens, J.M.; Wu, R. Systematic study of the dynamics and half-lives of newly synthesized proteins in human cells. *Chem. Sci.* **2016**, *7*, 1393–1400. [\[CrossRef\]](#) [\[PubMed\]](#)
56. Mirski, T.; Lidia, M.; Nakonieczna, A.; Gryko, R. Bacteriophages, phage endolysins and antimicrobial peptides—The possibilities for their common use to combat infections and in the design of new drugs. *Ann. Agric. Environ. Med.* **2019**, *26*, 203–209. [\[CrossRef\]](#) [\[PubMed\]](#)
57. Liu, J.; Chen, P.; Zheng, C.; Huang, Y.P. Characterization of maltocin P28, a novel phage tail-like bacteriocin from *Stenotrophomonas maltophilia*. *Appl. Environ. Microbiol.* **2018**, *79*, 5593–5600. [\[CrossRef\]](#) [\[PubMed\]](#)
58. Hockett, K.L.; Renner, T.; Baltrus, D.A. Independent Co-Option of a Tailed Bacteriophage into a Killing Complex in *Pseudomonas*. *mBio* **2015**, *6*, e00452. [\[CrossRef\]](#)
59. Oldfield, C.J.; Dunker, A.K. Intrinsically disordered proteins and intrinsically disordered protein regions. *Annu. Rev. Biochem.* **2014**, *83*, 553–584. [\[CrossRef\]](#)
60. Wright, P.E.; Dyson, H.J. Linking folding and binding. *Curr. Opin. Struct. Biol.* **2009**, *19*, 31–38. [\[CrossRef\]](#)

61. Takeda, K.; Miyatake, H.; Yokota, N.; Matsuyama, S.; Tokuda, H.; Miki, K. Crystal structures of bacterial lipoprotein localization factors, LolA and LolB. *EMBO J.* **2003**, *22*, 3199–3209. [[CrossRef](#)]
62. Ramamourthy, G.; Park, J.; Seo, C.; JVoegel, H.; Park, Y. Antifungal and Antibiofilm Activities and the Mechanism of Action of Repeating Lysine-Tryptophan Peptides against *Candida albicans*. *Microorganisms* **2020**, *8*, 758. [[CrossRef](#)]
63. Gasteiger, E.; Hoogland, C.; Gattiker, A.; Duvaud, S.; Wilkins, M.R.; Appel, R.D.; Bairoch, A. Protein Identification and Analysis Tools on the ExPASy Server. In *The Proteomics Protocols Handbook*; John, M.W., Ed.; Humana Press: Totowa, NJ, USA, 2005; pp. 571–607.
64. Kyte, J.; Doolittle, R.F. A simple method for displaying the hydropathic character of a protein. *J. Mol. Biol.* **1982**, *157*, 105–132. [[CrossRef](#)]
65. Wang, G.; Li, X.; Wang, Z. APD2: The updated antimicrobial peptide database and its application in peptide design. *Nucleic Acids Res.* **2009**, *37*, D933–D937. [[CrossRef](#)] [[PubMed](#)]
66. Wimley, W.C.; White, S.H. Experimentally determined hydrophobicity scale for proteins at membrane interfaces. *Nat. Struct. Biol.* **1996**, *3*, 842–848. [[CrossRef](#)] [[PubMed](#)]
67. Bailey, T.L.; Boden, M.; Buske, F.A.; Frith, M.; Grant, C.E.; Clementi, L.; Ren, J.; Li, W.W.; Noble, W.S. MEME SUITE: Tools for motif discovery and searching. *Nucleic Acids Res.* **2009**, *37*, W202–W208. [[CrossRef](#)]
68. Chen, C.P.; Kerynsky, A.; Rost, B. Transmembrane helix predictions revisited. *Protein Sci. A Publ. Protein Soc.* **2002**, *11*, 2774–2791. [[CrossRef](#)]
69. Krogh, A.; Larsson, B.; von Heijne, G.; Sonnhammer, E.L. Predicting transmembrane protein topology with a hidden Markov model: Application to complete genomes. *J. Mol. Biol.* **2001**, *305*, 567–580. [[CrossRef](#)]
70. Horton, P.; Nakai, K. Better Prediction of Protein Cellular Localization Sites with it k Nearest Neighbors Classifier. In Proceedings of the International Conference on Intelligent Systems for Molecular Biology, Halkidiki, Greece, 21–26 June 1997; Volume 5, pp. 147–152.
71. Kurgan, L.A.; Razib, A.A.; Aghakhani, S.; Dick, S.; Mizianty, M.J.; Jahandideh, S. CRYSTALP2: Sequence-based protein crystallization propensity prediction. *BMC Struct. Biol.* **2009**, *9*, 50. [[CrossRef](#)]
72. Mizianty, M.J.; Kurgan, L.A. Sequence-based prediction of protein crystallization, purification, and production propensity. *Bioinformatics* **2011**, *27*, i24–i33. [[CrossRef](#)]
73. Ashkenazy, H.; Abadi, S.; Martz, E.; Chay, O.; Mayrose, I.; Pupko, T.; Ben-Tal, N. Con Surf 2016: An improved methodology to estimate and visualize evolutionary conservation in macromolecules. *Nucleic Acids Res.* **2016**, *44*, W344–W350. [[CrossRef](#)]
74. Dereeper, A.; Guignon, V.; Blanc, G.; Audic, S.; Buffet, S.; Chevenet, F.; Dufayard, J.F.; Guindon, S.; Lefort, V.; Lescot, M.; et al. Phylogeny.fr: Robust phylogenetic analysis for the non-specialist. *Nucleic Acids Res.* **2008**, *36*, W465–W469. [[CrossRef](#)]
75. Buchan, D.W.A.; Jones, D.T. The PSIPRED Protein Analysis Workbench: 20 years on. *Nucleic Acids Res.* **2019**, *47*, W402–W407. [[CrossRef](#)] [[PubMed](#)]
76. Combet, C.; Blanchet, C.; Geourjon, C.; Deléage, G. NPS@: Network protein sequence analysis. *Trends Biochem. Sci.* **2000**, *25*, 147–150. [[CrossRef](#)]
77. King, R.D.; Sternberg, M.J. Identification and application of the concepts important for accurate and reliable protein secondary structure prediction. *Protein Sci.* **1996**, *5*, 2298–2310. [[CrossRef](#)] [[PubMed](#)]
78. Guermeur, Y.; Geourjon, C.; Gallinari, P.; Deléage, G. Improved performance in protein secondary structure prediction by inhomogeneous score combination. *Bioinformatics* **1999**, *15*, 413–421. [[CrossRef](#)] [[PubMed](#)]
79. Rost, B.; Sander, C. Prediction of protein secondary structure at better than 70% accuracy. *J. Mol. Biol.* **1993**, *232*, 584–599. [[CrossRef](#)] [[PubMed](#)]
80. Frishman, D.; Argos, P. Incorporation of non-local interactions in protein secondary structure prediction from the amino acid sequence. *Protein Eng.* **1996**, *9*, 133–142. [[CrossRef](#)]
81. Geourjon, C.; Deléage, G. SOPMA: Significant improvements in protein secondary structure prediction by consensus prediction from multiple alignments. *Comput. Appl. Biosci. CABIOS* **1995**, *11*, 681–684. [[CrossRef](#)]
82. Levin, J.M.; Robson, B.; Garnier, J. An algorithm for secondary structure determination in proteins based on sequence similarity. *FEBS Lett.* **1985**, *205*, 303–308. [[CrossRef](#)]
83. Deléage, G.; Blanchet, C.; Geourjon, C. Protein structure prediction. Implications for the biologist. *Biochimie* **1997**, *79*, 681–686. [[CrossRef](#)]
84. Biegert, A.; Mayer, C.; Remmert, M.; Söding, J.; Lupas, A.N. The MPI Bioinformatics Toolkit for protein sequence analysis. *Nucleic Acids Res.* **2006**, *34*, W335–W339. [[CrossRef](#)]
85. Fiser, A.; Sali, A. Modeller: Generation and refinement of homology-based protein structure models. *Methods Enzymol.* **2003**, *374*, 461–491. [[CrossRef](#)] [[PubMed](#)]
86. Kelley, L.A.; Sternberg, M.J. Protein structure prediction on the Web: A case study using the Phyre server. *Nat. Protoc.* **2009**, *4*, 363–371. [[CrossRef](#)] [[PubMed](#)]
87. Källberg, M.; Wang, H.; Wang, S.; Peng, J.; Wang, Z.; Lu, H.; Xu, J. Template-based protein structure modeling using the RaptorX web server. *Nat. Protoc.* **2012**, *7*, 1511–1522. [[CrossRef](#)] [[PubMed](#)]
88. Bairoch, A.; Apweiler, R. The SWISS-PROT protein sequence database and its supplement TrEMBL in 2000. *Nucleic Acids Res.* **2000**, *28*, 45–48. [[CrossRef](#)] [[PubMed](#)]

89. Wu, S.; Zhang, Y. LOMETS: A local meta-threading-server for protein structure prediction. *Nucleic Acids Res.* **2007**, *35*, 3375–3382. [[CrossRef](#)]
90. Yang, J.; Yan, R.; Roy, A.; Xu, D.; Poisson, J.; Zhang, Y. The I-TASSER Suite: Protein structure and function prediction. *Nat. Methods* **2015**, *12*, 7–8. [[CrossRef](#)]
91. Yang, Y.; Faraggi, E.; Zhao, H.; Zhou, Y. Improving protein fold recognition and template-based modeling by employing probabilistic-based matching between predicted one-dimensional structural properties of query and corresponding native properties of templates. *Bioinformatics* **2011**, *27*, 2076–2082. [[CrossRef](#)]
92. Kim, D.E.; Chivian, D.; Baker, D. Protein structure prediction and analysis using the Robetta server. *Nucleic Acids Res.* **2004**, *32*, W526–W531. [[CrossRef](#)]
93. Xu, D.; Zhang, Y. Ab initio protein structure assembly using continuous structure fragments and optimized knowledge-based force field. *Proteins* **2012**, *80*, 1715–1735. [[CrossRef](#)]
94. Jumper, J.; Evans, R.; Pritzel, A.; Green, T.; Figurnov, M.; Ronneberger, O.; Tunyasuvunakool, K.; Bates, R.; Žídek, A.; Potapenko, A.; et al. Highly accurate protein structure prediction with AlphaFold. *Nature* **2021**, *596*, 583–589. [[CrossRef](#)]
95. Mirdita, M.; Ovchinnikov, S.; Steinegger, M. ColabFold: Making protein folding accessible to all. *bioRxiv* **2021**, *8*, 9939. [[CrossRef](#)]
96. Laskowski, R.A.; MacArthur, M.W.; Moss, D.S.; Thornton, J.M. PROCHECK—A program to check the stereochemical quality of protein structures. *J. Appl. Cryst.* **1993**, *26*, 283–291. [[CrossRef](#)]
97. Benkert, P.; Biasini, M.; Schwede, T. Toward the estimation of the absolute quality of individual protein structure models. *Bioinformatics* **2011**, *27*, 343–350. [[CrossRef](#)]
98. Yang, J.; Roy, A.; Zhang, Y. Protein–ligand binding site recognition using complementary binding-specific substructure comparison and sequence profile alignment. *Bioinformatics* **2013**, *29*, 2588–2595. [[CrossRef](#)]
99. Ishida, T.; Kinoshita, K. PrDOS: Prediction of disordered protein regions from amino acid sequence. *Nucleic Acids Res.* **2007**, *35*, W460–W464. [[CrossRef](#)] [[PubMed](#)]
100. Prilusky, J.; Feder, C.E.; Zeev-Ben-Mordehai, T.; Rydberg, E.; Man, O.; Beckman, J.S.; Silman, I.; Sussman, J.L. FoldIndex: A simple tool to predict whether a given protein sequence is intrinsically unfolded. *Bioinformatics* **2005**, *21*, 3435–3438. [[CrossRef](#)] [[PubMed](#)]